Electrochemically enhanced wetting of 3YSZ and Mn1.5Co1.5O4 by AgCuO and their application in flash joining

Electrochemically enhanced wetting of 3YSZ and $Mn_{1.5}Co_{1.5}O_4$ by Ag–CuO and their application in flash joining

Yue Cao [a, b*], Guo-Cheng Xu [b], Elisa Zanchi [a*], Federico Smeacetto [a]

[a] Department of Applied Science and Technology, Politecnico di Torino, Corso Duca degli Abruzzi 24, Torino 10129, Italy

[b] Key Laboratory of Automobile Materials (Ministry of Education), Department of Materials Science and Engineering, Jilin University, No. 5988 Renmin Street, Changchun, 130025 PR China

*Corresponding author. E–mail address: yue.cao@polito.it, Tel./Fax.: +39 342–043–6820 (Yue Cao); elisa.zanchi@polito.it, Tel./Fax.: +39 338–461–0095 (Elisa Zanchi)

Abstract

Ag–CuO is a widely used air braze sealant for joining ceramic electrolytes and stainless-steel interconnects in solid oxide fuel cells (SOFCs). Balancing the amount of CuO in a braze is challenging because it enhances wettability and also aggravates steel surface degradation. Manganese cobaltite spinel (MCO) is widely used as a protective coating for SOFC steel interconnects. Therefore, we herein propose a strategy for enhancing the wetting of an Ag–CuO alloy with a low concentration of CuO (4 mol%) on 3 mol% yttria-stabilized zirconia (3YSZ) and MCO by applying a direct current to the 3YSZ/Ag–CuO/MCO system. It was discovered that the wetting of 3YSZ improved regardless of the current polarity; however, the wetting of MCO was selectively improved by the current flowing from MCO to 3YSZ. The underlying mechanisms are discussed based on the current-induced interfacial electrochemical reactions and dissolution. Furthermore, the flash joining of 3YSZ to MCO-coated Crofer22APU was achieved, and an optimized shear strength of 62 ± 11 MPa was obtained. A

correlation between the interfacial microstructure, mechanical properties, current polarity and current intensity was also established.

Key words: Solid oxide cell; Flash joining; Reactive air brazing; Metal/oxides interface.

1. Introduction

The combustion of fossil fuels, such as oil, coal and natural gas, produces large amounts of greenhouse gases. Societies worldwide are transforming their energy networks to gradually deviate from the use of fossil fuels. Solid oxide cell (SOC) devices are of great interest because of their high efficiency as either clean power generators (solid oxide fuel cells (SOFCs)) or converters of surplus renewable electricity to green hydrogen through electrolysis (solid oxide electrolysis cells (SOECs)), which can then be transformed into synthetic clean fuels and chemicals [1]. The core of the SOC technology is the stack, where several cells are typically mounted together via stainless-steel interconnects (ICs) to produce a usable power output. The planar stack configuration requires the sealing of the cells and the ICs to ensure gas tightness for thousands of h under severe SOC working conditions (650–850 °C in both reducing and oxidizing atmospheres). One of the main issues affecting the working life of the stack is the degradation of the sealing material at the interface with the ICs. Therefore, it is necessary to develop a strategy that simultaneously overcomes the problems with joining and material degradation [2, 3].

Reactive air brazing (RAB) has recently been developed as a method for joining electrolytes to steel ICs. The brazing material is usually made with a noble metal and an oxide compound to improve wettability. To date, Ag-based brazes with added oxide components such as CuO [4–6], Nb_2O_5 [7] and $CuAlO_2$ [8] are the most investigated brazes. However, the addition of these oxide components can

result in unfavorable interfacial reactions on the steel side. For example, the addition of 8 mol% CuO to Ag resulted in significant steel oxidation phenomena and the formation of Fe–Cr–Cu spinel oxides with thicknesses of 10–20 μm, which compromised the integrity of the joints [9]. This makes it significantly challenging to achieve both optimal wettability and chemical stability within the joint.

Our group has established an electric field-assisted technique that can largely improve the wettability of oxide ionic conductors using component-free metallic brazes. This technology has been used to improve the wetting of 3 mol% yttria-stabilized zirconia (3YSZ) by metals/alloys, such as Al [10], Cu [11] and 72Ag–28Cu [12], and to rapidly vacuum braze 3YSZ to Ni-based alloys [13] and steel [12]. However, the low oxidation resistance of these metals/alloys makes these joints unsuitable for use in high-temperature oxidizing environments (e.g., SOCs). More recently, Yue et al. achieved robust flash joining of 3YSZ to 430 ferritic stainless steel using an oxygen-resistant Ag–CuO braze [14]. The combination of electric field-induced Joule heating and electrochemical reactions aided in reducing the furnace temperature and time to 875 °C and 30 s, respectively, and substantially suppressing the growth of Fe–Cr–Cu spinel oxides. However, considering the high solubility of oxygen in Ag (1.93 mL at 1000 °C [15]), it is still challenging to maintain optimal mechanical and electrical performance for steel in direct contact with Ag in high-temperature oxidizing environments.

Regardless of the sealing material, stainless-steel ICs undergo continuous oxidation, which results in the thickening of the chromia scale and the evaporation of volatile Cr-species [16]. The use of ceramic protective coatings has been widely proposed to reduce chromium evaporation and excessive growth of the oxide scale [17]. Materials such as $La_{1-x}Sr_xMnO_3$ [18], $La_{1-x}Sr_xCoO_3$ [18], Al_2O_3 [19] and Mn–Co spinel [20] have been investigated. Among them, Mn–Co spinel is considered

a candidate for electric field-assisted processing technologies because it exhibits outstanding Cr barrier ability, a suitable coefficient of thermal expansion [20–22], excellent high-temperature conductivity (up to 60 S/cm) and excellent chemical stability (Co^{3+} transforms into Co^{2+} at temperatures above 1080 °C under an electric filed [23]). However, there are limited studies on the influence of electric fields on the wettability of Mn–Co spinel by metallic brazes. Additionally, the traditional sessile drop method is technically unable to reflect the wetting behavior when a joining system involves two ceramic phases on the top and bottom of the braze.

In this study, we developed a method that enables direct current (DC) to flow through ceramic/metal/ceramic interfaces and also investigated the impact of DC on the wettability of 3YSZ and Mn–Co spinel by an Ag–4mol%CuO alloy. Our findings revealed that the application of DC enhanced the wettability on the 3YSZ side regardless of polarity, but the wettability on the Mn–Co spinel side was enhanced only when the current flowed from Mn–Co spinel to 3YSZ. These findings led to the successful flash joining of 3YSZ to Mn–Co spinel-coated Crofer22APU steel, as well as the establishment of a correlation between the interfacial microstructure, mechanical properties, current polarity and current intensity.

2. Materials and experimental procedures

2.1 Materials and sample preparation

Polycrystalline zirconia stabilized with 3 mol% yttria having a 99% theoretical density was used in this work. The sizes of the 3YSZ pieces used for the wetting and joining experiments were 15 mm × 15 mm × 1 mm and φ 6 mm × 4 mm, respectively. The contact surface was polished using diamond paste with a particle size of 0.5 μm and then ultrasonically cleaned. Commercial manganese cobaltite

$Mn_{1.5}Co_{1.5}O_4$ (MCO) spinel powders with a particle size of 1 μm were used to prepare substrates for the wetting test and suspensions for coating. MCO substrates were prepared by cold pressing, followed by conventional sintering at 1000 °C in the air for 4 h. The final dimension and relative density of the sintered MCO substrates were approximately φ 11 mm × 1 mm and 69 %, respectively. MCO coating was prepared on Crofer22APU steel (Cr = 23 wt%, Mn = 0.45 wt%, La = 0.1 wt%, Ti = 0.06 wt%, Si and Al < 0.05 wt%, and Fe = Bal; 15 mm × 15 mm × 0.5 mm) using the electrophoretic deposition method (see the supplementary materials for the detailed experimental procedure and characterization). To prepare the braze, commercial Ag powders (purity: 99.95 %; average particle size: 100 nm) were mixed with 4 mol% CuO powders (purity: 99.95 %; average particle size: 1 μm) in ethyl alcohol for 24 h and dried overnight. The mixture was uniaxially cold-pressed to form pellets (approximately φ 3 mm × 0.8 mm) and thin sheets (approximately φ 6 mm ×120 μm) for the wetting and joining experiments, respectively.

2.2 Electric field-assisted wetting and flash joining

A wetting device that can apply DC to solid/liquid/solid systems was developed (Fig. 1a). Two 0.8 mm-thick alumina spacers were placed between the 3YSZ and MCO substrates, and the Ag–4mol%CuO pellets were inserted in the middle of the gap. The assemblies were then placed between two Ni–Cr electrodes and heated to 1000 °C at a rate of 10 °C/min in air. Subsequently, a 30 V initial electric field with different pre-set current intensity limits (0–800 mA) was applied for 1 min. Finally, the assemblies were cooled to ambient temperature at a rate of 10 °C/min. For concreteness, we herein define the current flowing from 3YSZ to MCO as positive (labelled with '+'), and the current flowing in the opposite direction as negative (labelled with '−').

Based on the wetting results, flash joining was performed on a highly related system, 3YSZ/Ag–CuO/MCO-coated Crofer22APU (Fig. 1b). The samples were assembled between two Ni–Cr electrodes, and a load of ~150 g was applied to ensure physical contact. Thereafter, they were heated to 1000 °C at a rate of 10 °C/min. Subsequently, DC with an initial voltage of 50 V was applied, and the samples were kept for 30 s after the current reached pre-set limits (0–1000 mA). Finally, the samples were cooled to room temperature at a rate of 5 °C/min. Figs. 1d and 1e show typical changes in the voltage and current with time during the wetting and joining experiments, respectively.

2.3 Characterization

The phase composition of the sintered MCO pellets and fracture surface was identified using X-ray diffraction (XRD) analysis (Panalytical, Xpert3 MRD). The density of the sintered MCO pellets was determined from the physical dimensions and weight of the samples. A theoretical density of 6.099 g/cm^3 was used to calculate the relative density. The profiles of the wetting assemblies were captured using hot-stage microscopic analysis (Expert System Solution, Modena, Italy) at room temperature. The shear strength of the joints was measured using a universal material testing machine (SINTEC D/10) with a homemade testing apparatus (Fig. 1c) at a loading rate of 0.05 mm/min. The apparent shear strength was calculated by dividing the maximum recorded force by the joining area. The average of three measurements was presented. The interfacial microstructures and fracture surfaces were characterized using a field-emission scanning electron microscope (FESEM; SupraTM 40, Zeiss, Oberkochen, Germany) equipped with an energy dispersive spectrometer (EDS; Bruker, Germany).

3. Results

3.1 Effect of DC on wettability

Fig. 2a shows the effect of the current on the wetting behavior of the Ag–CuO droplet on 3YSZ and MCO. Without DC application, the contact angles for 3YSZ and MCO stabilized at 50° ± 4°and 47° ± 5°, respectively (Fig. 2b). When the positive current was increased, the contact angle on 3YSZ remained relatively stable initially before dropping to 32° ± 4° at +300 mA and finally reaching a minimum of 28° ± 3° at +400 mA. Nevertheless, when the current intensity reached +600 mA or higher, the contact angle scattered, the droplet shape became asymmetric (Fig. 2c) and the 3YSZ and MCO substrates fractured occasionally. These out-of-equilibrium phenomena can be related to the inhomogeneity of the temperature distribution near the triple line, similar to the inhomogeneous densification issue in flash sintering works [24]. Conversely, the contact angle on MCO slightly increased as the current increased from 0 mA to +400 mA, indicating that the positive current could not improve the wettability on the MCO side.

When the current was reversed (from MCO to 3YSZ), the contact angle on the 3YSZ side decreased to 31° ± 3° at a current of −50 mA (Fig. 2a). As the current increased, the contact angle reached a minimum of 27° ± 4° at −100 mA, similar to the value achieved under the positive current ($28^{o} \pm 3^{o}$). Notably, the contact angle on the MCO side also decreased as the current intensity increased, reaching 30° ± 4° at −100 mA. This demonstrates that a negative current can reduce the contact angle on both sides with low intensities. However, as the current reached −200 mA, the droplet became unstable and travelled to the edge of the substrates, and a blackening phenomenon occurred along the droplet trajectory on the other 3YSZ side (Fig. 2d), demonstrating current localization.

Fig. 3 illustrates the effect of current polarity and intensity on interfacial microstructure. Without

DC application, a CuO layer formed on both the 3YSZ and MCO surfaces (Figs. 3a_1–3a_3), and the Ag melt diffused into the MCO matrix, particularly in the region near the wetting front (Fig. 3a_2). However, there were still some unfilled pores at the interface (Fig. 3a_4), demonstrating poor wettability. When the current was increased to +100 mA, the CuO on both surfaces was eliminated, and the molten Ag drastically infiltrated the MCO matrix (Figs. 3b_2 and 3b_4). Moreover, a strong dissolution of 3YSZ occurred primarily inside the 3YSZ/Ag interface (Fig. 3b_1), which differs from the phenomenon observed in dissolutive metal/ceramics systems (where the dissolution is more uniform along the interface [25]). Nevertheless, there was no significant difference in the contact angle (stabilized at 52° ± 4°). As the current reached +400 mA, the dissolution phenomenon extended to the wetting front (Figs. 3c_1 and 3c_3), and the contact angle decreased to 28° ± 3° (Fig. 2a). These results indicate a relationship between 3YSZ dissolution and wettability enhancement.

Under a DC of −100 mA, no dissolution was observed at either interface. However, precursor film-like products were observed in front of the droplet (Fig. 3d_1). In traditional high-temperature wetting studies, precursor films develop spontaneously in metal/ceramic systems owing to the presence of active elements (such as Ti, Zr and Hf) [26]. However, no ‘precursor film’ was observed in the zero-current case (Fig. 3a_1) despite the presence of CuO adsorption (Fig. 3a_3). This implies that these substances were not generated spontaneously; instead, the negatively polarized current may have played a more important role. For further clarification, the top view of the triple line region was observed, and spot scanning was performed. Figs. 3d_4 and 3d_5 show that Ag and CuO were discretely distributed on the 3YSZ surface (Table 1), which contradicts the precursor film hypothesis. A more convincing explanation is that the droplet on the 3YSZ surface retracted during the processing. This

scenario agrees with the secondary spreading observed on the MCO side (Fig. 3d$_2$). The mechanism behind this unusual droplet behavior is discussed in section 4.

3.2 Flash joining

Fig. 4 shows the interfacial microstructural evolution of the joints prepared under both current polarities. In the zero-current case, seams and cracks were detected at the 3YSZ/Ag–CuO and Ag–CuO/MCO interfaces, respectively, which can be ascribed to poor wettability (Fig. 2a) and insufficient duration (30 s). For the joint obtained at +200 mA, both interfaces were well bonded, and the amount of CuO on the MCO surface was significantly reduced (Fig. 4b$_1$). Additionally, some small particles were detected in the Ag matrix near the MCO layer, which eventually coalesced into a 7 μm-thick layer over MCO as the current increased to +1000 mA (Fig. 4b$_3$). EDS point analysis confirmed that this layer was single stoichiometric ZrO_2, which agrees with the dissolution that occurred at the 3YSZ/Ag interface (Fig. 4b$_2$). These phenomena indicate that ZrO_2 dissolved into the Ag melt and then accumulated and coalesced on the MCO surface, resulting in the formation of a mixed layer (Fig. 4b$_3$), which embrittled the joint. In contrast, for the sample joined at −200 mA, both interfaces were well-bonded, and the Ag matrix had no ZrO_2 particles (Fig. 4c$_1$). However, when the current was increased to −1000 mA, some dark-grey phases were generated on the steel surface, rupturing the MCO layer (Fig. 4c$_2$). EDS analysis revealed that these phases mainly consisted of 46.69 at.% Cr and 45.58 at.% O (Fig. 4c$_3$), which could be identified as Cr-rich oxides. Hence, both positive and negative currents facilitated rapid joining; however, intense currents accelerated the growth of undesirable substances (ZrO_2 particles and Cr-rich oxides), causing the MCO layer to rupture.

Fig. 5a shows the effect of current intensity on the shear strength of joints obtained under a

positive current. Without DC application, the shear strength was only 6 ± 2 MPa, and the fracture exhibited a mixed mode comprising MCO and 3YSZ surfaces (Fig. 6a_1). The presence of pores inside the MCO indicated insufficient Ag melt infiltration (Fig. 6a_2), which is consistent with the wetting test (Fig. 3a_4). Additionally, a part of the 3YSZ surfaces remained in its original state (Fig. 6a_3), demonstrating weak bonding. As the current increased, the joint strength significantly increased to a maximum of 51 ± 10 MPa at +100 mA. A further increase to +1000 mA resulted in the weakening of the joints. The fracture mode in the samples joined under a positive current was similar to that in the zero-current case (Fig. 6a_1), but the MCO area dominated the surface (Fig. 6b_1), demonstrating that the positive current improved the bonding of 3YSZ/Ag interface. Fig. 6b_2 shows the fracture surface on the 3YSZ side of the joint prepared at +200 mA. In addition to Ag residuals, numerous rod-shaped grains with sizes varying from nanometer to micrometer were also detected (Fig. 6b_3). To identify these products, EDS and XRD analyses were both used. The EDS results revealed the formation of a single ZrO_2 phase (Fig. 6b_3); however, the XRD pattern detected both t-ZrO_2 (i.e., a typical 3YSZ phase) and m-ZrO_2, which has not been observed in our previous studies [10–14]. To better understand this finding, the XRD patterns for the fracture surfaces of the joints obtained from 0 to +400 mA were compared (Fig. 7). It was discovered that m-ZrO_2 existed only when the current intensity was ≥ +200 mA, indicating a relationship between m-ZrO_2 formation and the positive current.

Fig. 5b shows the effect of current intensity on the shear strength of the joints obtained under a negative polarity. As the current intensity increased, the shear strength initially increased to a maximum of 62 ± 11 MPa at −200 mA and then gradually decreased. An increase of ~44% was achieved when compared to the shear strength of the joint obtained under the same positive current

(43 ± 10 MPa at +200 mA). This implies that although flash joining was achieved under both polarities, the m-ZrO_2 particles formed under positive polarity were more unfavorable than the Cr-rich oxides (Fig. 4c_3), presumably because of their embrittlement effect on the Ag melt (Fig. 4b_1). Additionally, the poor wettability at the MCO side (Fig. 2a) also indicated a weak bonding at the Ag/MCO interface, thus resulting in a mixed fracture mode (Fig. 6b_1). In contrast, the fracture in the negative group occurred only within MCO (see Figs. 6c_1 and 6c_2). This was also confirmed by the XRD analysis (Fig. 7). According to the corresponding microstructure (Figs. 4c_2 and 4c_3), this type of fracture could be ascribed to the growth of Cr-rich oxides at the MCO/Crofer22APU interface, which increased the mechanical stress inside MCO.

4. Discussion

It is necessary to understand the intrinsic wetting mechanism of Ag–CuO before exploring the role of current in improving wettability. Thanaphong et al. [28] employed the density functional theory to calculate the work of adhesion (W_{ad}) of potential interfaces within the Ag–CuO/YSZ system and summarized that two primary mechanisms promote Ag to wet YSZ surface: (I) the formation of Ag–O clusters at Ag/YSZ interface from oxygen in the solution, and (II) enhanced W_{ad} due to the formation of a CuO scale on the YSZ surface. More specifically, the calculated W_{ad} of the Ag(l)/YSZ(111) and {Ag(l)+2O}/YSZ(111) interfaces were 0.11 J/m^2 and 0.43 J/m^2, respectively, resulting in theoretical contact angles of 149° and 111° (a 38° reduction), while the W_{ad} of the Ag[$\bar{3}$21](111)/YSZ[$\bar{1}$10](111) and Ag[1$\bar{1}$0](111)/CuO[$\bar{1}$10](111) interfaces were 0.10 J/m^2 and 0.48 J/m^2, respectively, resulting in contact angles of 150° and 112° (also a 38° reduction). The identical reduction in contact angle suggested that factors (I) and (II) contribute equally to wettability enhancement. However,

experimental evidence revealed that the presence of Ag–O clusters in the Ag/YSZ system reduced the contact angle from 120° [29] to 90° [30], whereas the addition of CuO significantly reduced it to 10° [31]. This deviation from the calculated results is attributable to the lack of dissolved oxygen at the Ag/YSZ interface, which was due to the low solubility of oxygen in Ag (1.93 mL at 1000 °C [15], i.e., ~1 mol%).

Based on the above analysis, a concept physical model was established to understand the electrochemical process of the wetting and joining activities (Fig. 8). According to the Ag–CuO binary phase diagram [4], a CuO-rich liquid was formed when the temperature exceeded 964 °C and was gradually adsorbed at both interfaces, resulting in a relative wetting state. Since silver is an excellent electron carrier, the adsorbed CuO would be reduced to Cu and dissolve into the Ag melt regardless of the current polarity. Hence, the Ag/3YSZ and Ag/MCO interfaces were primarily considered. Under positive polarization (Fig 8a), the lattice oxygen ($O_O^\times$) of 3YSZ migrated to the anode and was released in form of oxygen molecules:

$$O_O^\times \rightarrow V_O^{\cdot\cdot} + 2e' + \frac{1}{2}O_2 \qquad (1)$$

Correspondingly, positively charged oxygen vacancies ($V_O^{\cdot\cdot}$) travelled to the cathode and combined with the dissolved oxygen and electrons from the Ag melt, producing lattice oxygen ($O_O^\times$):

$$V_O^{\cdot\cdot} + 2e' + \frac{1}{2}O_2 \rightarrow O_O^\times \qquad (2)$$

However, as the current intensity increased, the dissolved oxygen content (in Ag) was no longer sufficient to promote reaction (2), particularly at the center of the interface (where the oxygen partial pressure ($P(O_2)$) was lower than the droplet surface). In this case, the excess vacancies reacted with the ZrO_2 and electrons, forming sub-stoichiometric $ZrO_{2-\delta}$:

$$ZrO_2 + \delta V_O^{\cdot\cdot} + 2\delta e' \rightarrow ZrO_{2-\delta} + \delta O_O^{\times} \quad (3)$$

Since the Zr–O bonds in $ZrO_{2-\delta}$ are relatively weak, substantial Zr–Ag bonds could develop at the Ag/3YSZ interface, thereby reducing the solid/liquid interfacial free energy [11–13] and enhancing wetting and interfacial bonding. Owning to the different $P(O_2)$ along the interface, reactions (2) and (3) proceeded simultaneously at the edge and inside of the Ag droplet, respectively, causing a competition (Fig. 8b). Therefore, it is inferred that the Zr–Ag bonds could only significantly alter Young's equilibrium at the triple line when reaction (3) was dominant at the front of the droplet (i.e., when the current reached the threshold of +300 mA), which enabled rapid spreading of the droplet. The current threshold achieved in this study is two orders of magnitude higher than the values obtained in a high vacuum (e.g., a current as low as +1 mA could reduce the contact angle from 148° to 87° in Al/YSZ system [10]). Such difference reflects the presence of competition (between reactions (2) and (3)), which does not exist in high-vacuum systems. Another distinct phenomenon is the strong dissolution of 3YSZ into the Ag melt (Figs. 3b_3 and 4b_2). Such extensive dissolution has not been observed in wetting or brazing studies on Ag/YSZ or related systems because it is not thermodynamically spontaneous [8, 19, 32]. Generally, the dissolution of an oxide A_xO_y into metallic melt M is described as follows:

$$A_xO_y \rightarrow x[A]_M + y[O]_M \quad (4)$$

However, under a positive electric field, both oxygen in the 3YSZ lattice and molten Ag migrate towards the anode (Fig. 8b), significantly inhibiting the transfer of oxygen (from 3YSZ to Ag melt) indicated in reaction (4). Instead, lattice vacancies accumulate at the interface and react with electrons, accelerating the formation of Zr atoms and their diffusion towards the Ag melt. Owning to the high

solubility of Zr in Ag (8 at.% at 1000 °C [33]), the as-formed Zr will spontaneously dissolve in Ag, forming Ag-rich (Ag, Zr) liquid phase:

$$2ZrO_2 \xrightarrow{E\ field} [Zr]_{Ag} + ZrO_{2-\delta} + (2+\delta)[O]_{3YSZ} \quad (5)$$

Meanwhile, oxygen vacancies accumulated in 3YSZ and acted as diffusion path for the Ag melt, leading to a cyclic reaction at the front of the interface and the occurrence of a strong dissolution (Fig. 4b$_2$). Owing to the constant dissolution of oxygen from the atmosphere, Zr atoms were oxidized and coalesced with each other as the current was cut off, directly forming micron- and nano-sized yttria-free m-ZrO_2 crystals (according to ZrO_2-Y_2O_3 phase diagram [34]). This process can be described as an electric field-driven dissolution in the Ag/3YSZ system. For a traditional dissolution-driven wetting system, the energy barrier for spreading has three contributions [35]:

$$\Delta G_W = \Delta G_S + \Delta G_{vis} + \Delta G_{fusion} \quad (6)$$

where ΔG_S is the surface contribution, ΔG_{vis} is the viscous contribution and ΔG_{fusion} is the contribution by the heat of fusion. Although it is technically difficult to quantify the energy absorbed by the dissolution (reaction (5)), qualitatively, the application of the electric field converted the dissolution from intrinsically nonspontaneous to partially enabled (Zr atoms). In addition, the dissipated Joule heating increased the temperature of the Ag droplet via heat conduction, reducing the energy barrier in terms of viscosity [36]. For the ΔG_S, since the Ag–O cluster placed on the Ag-free surface yielded a W_{ad} of ~0 J/m^2 [28], the electrical reduction of the dissolved oxygen on the Ag surface did not inhibit wetting. Therefore, it can be concluded that the electric field-induced dissolution and $ZrO_{2-\delta}$ formation both contributed to the wettability enhancement. Regarding the MCO side, it should be noted that MCO conductivity follows a polaron hopping mechanism and is governed

by the hopping of oxidation states between the Co^{3+}/Co^{2+} and Mn^{4+}/Mn^{3+} pairs [23, 37, 38]. Therefore, the interfacial charge transition was dominated by electrons, and no visible chemical reactions or dissolution occurred at the Ag/MCO interface. The slight increase in the contact angle (Fig. 2a) could be attributed to the loss of oxygen at the Ag/MCO interface (consumed by reaction (2)), which suppressed the wetting through mechanism (Ⅰ).

Under negative polarization, reaction (1) occurred at the Ag/3YSZ interface, and the lattice oxygen migrated towards the Ag melt, generating dissolved oxygen:

$$ZrO_2 + [O]_{3YSZ} \xrightarrow{E\ field} ZrO_2 + [O]_{Ag} \quad (7)$$

The generated oxygen led to the formation of Ag–O clusters directly at the 3YSZ/Ag interface (Fig. 8c), significantly promoting wetting through mechanism (Ⅰ). Moreover, driven by reaction (3), oxygen from the atmosphere entered the 3YSZ lattice from the cathode, continuously supplying oxygen for reaction (7). As the duration increased, the oxygen at the 3YSZ/Ag interface became supersaturated and diffused towards MCO, increasing the concentration of Ag–O clusters on the MCO surface (Fig. 8d) and consequently enhancing wettability and interfacial joining. However, the presence of open pores inside the MCO coating resulted in a direct contact between the oxygen-rich Ag and the steel surface, causing an overgrowth of the Cr-rich oxides (Fig. 4c_3). With further increases of current, the generated oxygen could no longer completely dissolve into the Ag melt. Hence, these undissolved oxygen molecules accumulated into bubbles and escaped from the droplet, causing a random droplet motion (Fig. 2d). As the current was cut off, the state of the Ag–O clusters at the Ag/3YSZ interface gradually transitioned from supersaturation to equilibrium, and correspondingly, the droplet on the 3YSZ surface retracted to produce precursor film-like residuals in the wetting front

(Figs. 3d_4 and 3d_5).

5. Conclusions

1. The application of DC to a 3YSZ/Ag–4mol%CuO/MCO system promotes the wetting of Ag–4mol%CuO on 3YSZ regardless of the current polarity. However, the wetting of MCO can be promoted when the current flows from MCO to 3YSZ.

2. When the current flowed from 3YSZ to MCO, the wetting of 3YSZ was facilitated by the formation of sub-stoichiometric $ZrO_{2-\delta}$ and its dissolution at the interface. The current threshold for achieving this is up to 300 mA, which is two orders of magnitude higher than that observed in a vacuum system. This is due to the involvement of oxygen from air in interfacial electrochemical reactions, which inhibits the formation of $ZrO_{2-\delta}$ and dissolution. The wetting of MCO was slightly inhibited due to the loss of dissolved oxygen at the Ag/MCO interface.

3. When the current flowed from MCO to 3YSZ, the current-induced dissociation of lattice oxygen from 3YSZ facilitated the formation of Ag–O clusters at both interfaces, thereby promoting wetting on both sides. The current threshold for achieving this is as low as 50 mA. This approach is potentially a versatile method that enhances the wettability of Ag-based brazes on various oxides.

4. The flash joining of 3YSZ to MCO-coated Crofer22APU steel was achieved using a DC-driven electrochemical technique. The shear strength of the joints initially increased and then decreased with increasing current intensity for both polarities. Maximum shear

strengths of 51 ± 10 MPa and 62 ± 11 MPa were obtained at +100 mA and −200 mA, respectively, for the positive and negative current groups. The formation of m-ZrO_2 grains and the overgrowth of Cr-rich oxides were determined as the factors deteriorating the joint for the positive and negative high-current intensity cases, respectively.

Acknowledgments

Y. Cao is grateful to the China Scholarship Council (CSC) for funding of Ph.D. scholarship (No. 202106170081).

References:

[1] S.M. Haile, Fuel cell materials and components, Acta Mater. 51 (2003) 5981–6000. https://doi.org/10.1016/j.actamat.2003.08.004

[2] P.A. Lessing, A review of sealing technologies applicable to solid oxide electrolysis cells, J. Mater. Sci. 42 (2007) 3465–3476. https://doi.org/10.1007/s10853-006-0409-9

[3] J.W. Fergus, Sealants for solid oxide fuel cells, J. Power Sources. 147 (2005) 46–57. https://doi.org/10.1016/j.jpowsour.2005.05.002

[4] J.R. Friant, A. Meier, J.T. Darsell, K.S. Weil, Transitions in wetting behavior between liquid Ag–CuO alloys and Al_2O_3 substrates, J. Am. Ceram. Soc. 95 (2012) 1549–1555. https://doi.org/10.1111/j.1551-2916.2012.05094.x

[5] J.Y. Kim, J.S. Hardy, K.S. Weil, Effects of CuO content on the wetting behavior and mechanical properties of a Ag–CuO braze for ceramic joining, J. Am. Ceram. Soc. 88 (2005) 2521–2527. https://doi.org/10.1111/j.1551-2916.2005.00492.x

[6] S. Le, Z. Shen, X. Zhu, X.L. Zhou, Y. Yan, K. Sun, N. Zhang, Y.X. Yuan, Y. Mao, Effective Ag–

CuO sealant for planar solid oxide fuel cells, J. Alloys Compd. 496 (2010) 96–99. https://doi.org/10.1016/j.jallcom.2010.01.131

[7] Z. Sun, L.X. Zhang, X. Li, S.S. Zhang, Reactive air brazing of the YSZ/AISI 310s couples using a novel Ag–Nb_2O_5 sealant, Ceram. Int. 46 (2020) 5168–5174, https://doi.org/10.1016/j.ceramint.2019.10.262

[8] L. Chen, C. Li, X. Si, X. Wang, Z. Wang, J. Cao, A novel Ag–$CuAlO_2$ sealant for reactive air brazing of 3YSZ and AISI 310S, Ceram. Int. 47 (2021) 31413–31422. https://doi.org/10.1016/j.ceramint.2021.08.017

[9] B. Kuhn, F.J. Wetzel, J. Malzbender, R.W. Steinbrech, L. Singheiser, Mechanical performance of reactive-air-brazed (RAB) ceramic/metal joints for solid oxide fuel cells at ambient temperature, J. Power Sources 193 (2009) 199–202, https://doi. org/10.1016/j.jpowsour.2008.10.117

[10] N. Yang, P. Shen, B. Yang, R. fen Guo, Q. chuan Jiang, Significant improvement in the wettability of ZrO_2 by molten Al under the application of a direct current, Mater. Des. 111 (2016) 158–163. https://doi.org/10.1016/j.matdes.2016.08.081

[11] L.T. Yu, P. Shen, B. Yang, R.F. Guo, N. Zhang, Q.C. Jiang, Polarity effects on the wettability and interfacial chemistry at Cu–YSZ interface by applying a direct current, J. Eur. Ceram. Soc. 38 (2018) 1790–1795. https://doi.org/10.1016/j.jeurceramsoc.2017.10.049

[12] L. Li, C. Wei, P. Shen, Q.C. Jiang, DC-assisted rapid wetting of 3Y-PSZ by molten 72Ag–28Cu and its application in joining, J. Eur. Ceram. Soc. 39 (2019) 2132–2139. https://doi.org/10.1016/j.jeurceramsoc.2019.01.046

[13] L. Li, L.-T. Yu, Y.-Z. Liang, L. Zhao, S.-B. Jin, P. Shen, Electrochemical wetting of 3YSZ by Cu

and ultrafast joining with a Ni-based superalloy, J. Eur. Ceram. Soc. 42 (2021) 1113–1120. https://doi.org/10.1016/j.jeurceramsoc.2021.11.007

[14] Y. Cao, G.C. Xu, P. Shen, Flash joining of 3YSZ and 430 SS using Ag–CuO filler, Ceram. Int. 48 (2022) 4005–4014. https://doi.org/10.1016/j.ceramint.2021.10.187

[15] F.G. Donnan, T.W.A. Shaw, The solubility of oxygen in molten silver, J. Soc. Chem. Ind 29 (1910) 987–989. https://doi.org/10.1002/jctb.5000291602

[16] J.C.W. Mah, A. Muchtar, M.R. Somalu, M.J. Ghazali, Metallic interconnects for solid oxide fuel cell: A review on protective coating and deposition techniques, Int. J. Hydrogen Energy. 42 (2017) 9219–9229. https://doi.org/10.1016/j.ijhydene.2016.03.195.

[17] N. Shaigan, W. Qu, D.G. Ivey, W. Chen, A review of recent progress in coatings, surface modifications and alloy developments for solid oxide fuel cell ferritic stainless steel interconnects, J. Power Sources. 195 (2010) 1529–1542. https://doi.org/10.1016/j.jpowsour.2009.09.069

[18] M. Stanislowski, J. Froitzheim, L. Niewolak, W.J. Quadakkers, K. Hilpert, T. Markus, L. Singheiser, Reduction of chromium vaporization from SOFC interconnectors by highly effective coatings, J. Power Sources. 164 (2007) 578–589. https://doi.org/10.1016/j.jpowsour.2006.08.013

[19] W.L. Zhou, S.P. Hu, M.J. Yang, Y. Luo, W. Fu, X.G. Song, Reactive air brazing of 3YSZ ceramic to aluminized Crofer22H stainless steel using Ag–CuO fillers, Int. J. Appl. Ceram. Technol. 19 (2022) 2367–2378. https://doi.org/10.1111/ijac.14035

[20] E. Zanchi, J. Ignaczak, S. Molin, G. Cempura, A.R. Boccaccini, F. Smeacetto, Electrophoretic co-deposition of $Mn_{1.5}Co_{1.5}O_4$, Fe_2O_3 and CuO: Unravelling the effect of simultaneous addition of Cu and Fe on the microstructural, thermo-mechanical and corrosion properties of in-situ modified spinel

coatings for solid oxide cell intercon, J. Eur. Ceram. Soc. 42 (2022) 3271–3281. https://doi.org/10.1016/j.jeurceramsoc.2022.02.008

[21] X. Wang, X. Si, J. Gao, B. Yang, M. Li, C. Li, J. Qi, J. Cao, Effects of the Mn–Co spinel coating on $BaZr_{0.1}Ce_{0.7}Y_{0.1}Yb_{0.1}O_{3-\delta}$/AISI 441 reactive air brazed joint: Microstructure, strength, and stability, Ceram. Int. 49 (2022) 5154–5160. https://doi.org/10.1016/j.ceramint.2022.10.032

[22] A.G. Sabato, E. Zanchi, S. Molin, G. Cempura, H. Javed, K. Herbrig, C. Walter, A.R. Boccaccini, F. Smeacetto, Mn-Co spinel coatings on Crofer 22 APU by electrophoretic deposition: Up scaling, performance in SOFC stack at 850 °C and compositional modifications, J. Eur. Ceram. Soc. 41 (2021) 4496–4504. https://doi.org/10.1016/j.jeurceramsoc.2021.03.030

[23] A. Gaur, V.M. Sglavo, Flash-sintering of $MnCo_2O_4$ and its relation to phase stability, J. Eur. Ceram. Soc. 34 (2014) 2391–2400. https://doi.org/10.1016/j.jeurceramsoc.2014.02.012

[24] G.M. Jones, M. Biesuz, W. Ji, S.F. John, C. Grimley, C. Manière, C.E.J. Dancer, Promoting microstructural homogeneity during flash sintering of ceramics through thermal management, MRS Bull. 46 (2021) 59–66. https://doi.org/10.1557/s43577-020-00010-2

[25] T.J. Singler, S. Su, L. Yin, B.T. Murray, Modeling and experiments in dissolutive wetting: A review, J. Mater. Sci. 47 (2012) 8261–8274. https://doi.org/10.1007/s10853-012-6622-9

[26] Q. Lin, L. Liu, W. Zhu, Formation Mechanism of Precursor Films at High Temperatures: A Review, Chinese J. Mech. Eng. (English Ed. 35 (2022). https://doi.org/10.1186/s10033-022-00686-4

[27] N. Morisaki, H. Yoshida, T. Tokunaga, K. Sasaki, T. Yamamoto, Consolidation of undoped, monoclinic zirconia polycrystals by flash sintering, J. Am. Ceram. Soc. 100 (2017) 3851–3857. https://doi.org/10.1111/jace.14954

[28] T. Phongpreecha, J.D. Nicholas, T.R. Bieler, Y. Qi, Computational design of metal oxides to enhance the wetting and adhesion of silver-based brazes on yttria-stabilized-zirconia, Acta Mater. 152 (2018) 229–238. https://doi.org/10.1016/j.actamat.2018.04.024

[29] P. Nikolopoulos, G. Ondracek, D. Sotiropoulou, Wettability and interfacial energies between zirconia ceramic and liquid metals, Ceram. Int. 15 (1989) 201–206. https://doi.org/10.1016/0272-8842(89)90039-4

[30] J.T. Darsell, K.S. Weil, Experimental determination of phase equilibria in the silver-copper oxide system at high temperature, Scr. Mater 56 (2007) 1111–1114. https://doi.org/10.1016/j.scriptamat.2007.01.050

[31] K.S. Weil, J.Y. Kim, J.S. Hardy, Reactive air brazing: a novel method of sealing sofcs and other solid-state electrochemical devices, Electrochem. Solid-State Lett. 8 (2005) A133–A136. http://doi.org/10.1149/1.1850391

[32] J.Y. Kim, J.S. Hardy, K.S. Weil, Silver-copper oxide based reactive air braze for joining yttria-stabilized zirconia, J. Mater. Res. 20 (2005) 636–643. https://doi.org/10.1557/JMR.2005.0088

[33] D.H. Kang, I.H. Jung, Critical thermodynamic evaluation and optimization of the Ag-Zr, Cu-Zr and Ag-Cu-Zr systems and its applications to amorphous Cu-Zr-Ag alloys, Intermetallics. 18 (2010) 815–833. https://doi.org/10.1016/j.intermet.2009.12.013

[34] H.G. Scott, Phase relationships in the zirconia-yttria system, J. Mater. Sci. 10 (1975) 1527–1535. https://doi.org/10.1007/BF01031853.

[35] L. Yin, Reactive Wetting and Spreading in Binary Metallic Systems, Ph.D thesis, Binghamton University, New York, 2005

[36] O.K. Echendu, E.C. Mbamala, B.C. Anusionwu, Theoretical investigation of the viscosity of some liquid metals and alloys, Phys. Chem. Liq. 49 (2011) 247–258. https://doi.org/10.1080/00319100903539520

[37] V. Massarotti, D. Capsoni, M. Bini, G. Chiodelli, C.B. Azzoni, M.C. Mozzati, a Paleari, Electric and Magnetic Properties of $LiMn_2O_4$-and Li_2MnO_3-Type Oxides, Jounal Solid State Chem. 100 (1997) 94–100. https://doi.org/10.1006/jssc.1997.7349

[38] H. Bordeneuve, A. Rousset, C. Tenailleau, S. Guillemet-Fritsch, Cation distribution in manganese cobaltite spinels $Co_{3-x}Mn_xO_4$ ($0 \leq x \leq 1$) determined by thermal analysis, J. Therm. Anal. Calorim. 101 (2010) 137–142. https://doi.org/10.1007/s10973-009-0557-7

Figure Captions

Fig. 1. Schematics of the electric field-assisted (a) wetting and (b) flash joining devices. (c) Schematic of the shear test apparatus. Typical changes in the voltage and current with time during the (d) wetting and (e) flash joining experiments.

Fig. 2. (a) Variations in the final contact angle with current intensities and polarities for molten Ag–4mol%CuO situated between 3YSZ and MCO substrates. Droplet profiles under different current intensities of (b) 0 mA and (c) 200–800 mA in a positive polarity and (d) 50–200 mA in a negative polarity (the inset shows the localized current path). The profiles are in the order of 3YSZ/Ag–CuO/MCO, from top to bottom. (e) A typical photograph of the wetting sample.

Fig. 3. Microstructures at both wetting fronts (the 3YSZ and MCO sides) and the internal interfaces for the samples tested under different current intensities: (a_1–a_4) 0 mA, (b_1–b_4) +100 mA, (c_1–c_4) +400 mA and (d_1–d_5) −100 mA.

Fig. 4. Cross-sectional micrographs of the 3YSZ/Ag–CuO/MCO-coated Crofer22APU joints prepared at 1000 °C under different current intensities: (a_1–a_3) 0 mA, (b_1) +200 mA, (b_2, b_3) +1000 mA, (c_1) −200 mA and (c_2, c_3) −1000 mA.

Fig. 5. Shear strength of the joints obtained at different current intensities under (a) positive and (b) negative polarities (furnace temperature: 1000 °C; holding time: 30 s).

Fig. 6. Fracture surfaces of the joints prepared at current intensities of (a_1, a_2, a_3) 0 mA, (b_1, b_2, b_3) +200 mA and (c_1, c_2) −200 mA.

Fig. 7. XRD patterns of the fracture surfaces of the 3YSZ side in the joints prepared at 0 mA, +50 mA, +200 mA, +400 mA, −50 mA and −200 mA.

Fig. 8. Schematic representation of the electrochemical reaction in the 3YSZ/Ag–CuO/MCO system during wetting under the application of (a, b) positive and (c, d) negative DC.

Table

Table 1. Chemical compositions and possible phases marked in **Fig. 3**.

Spots	Ag	Zr	Cu	O	Phase
A	0.1	-	39.6	60.4	CuO
B	98.6	1.4	-	-	Ag
C	91.1	0.2	0.3	8.4	Ag
D	-	0.3	40.0	59.7	CuO
E	-	36.9	-	63.1	ZrO_2

Figure 1

Click here to access/download;Figure;Fig. 1.jpg

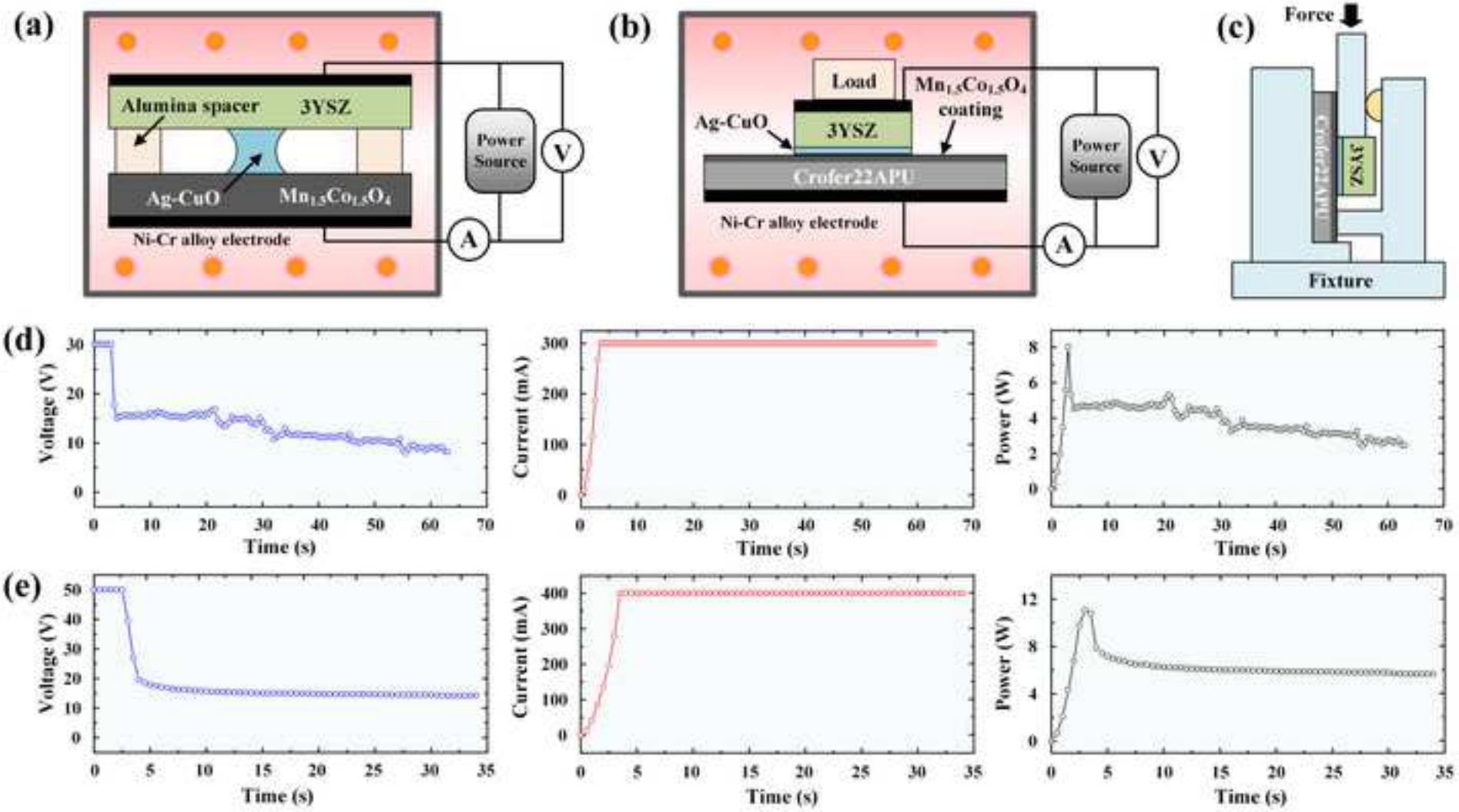

Figure 2

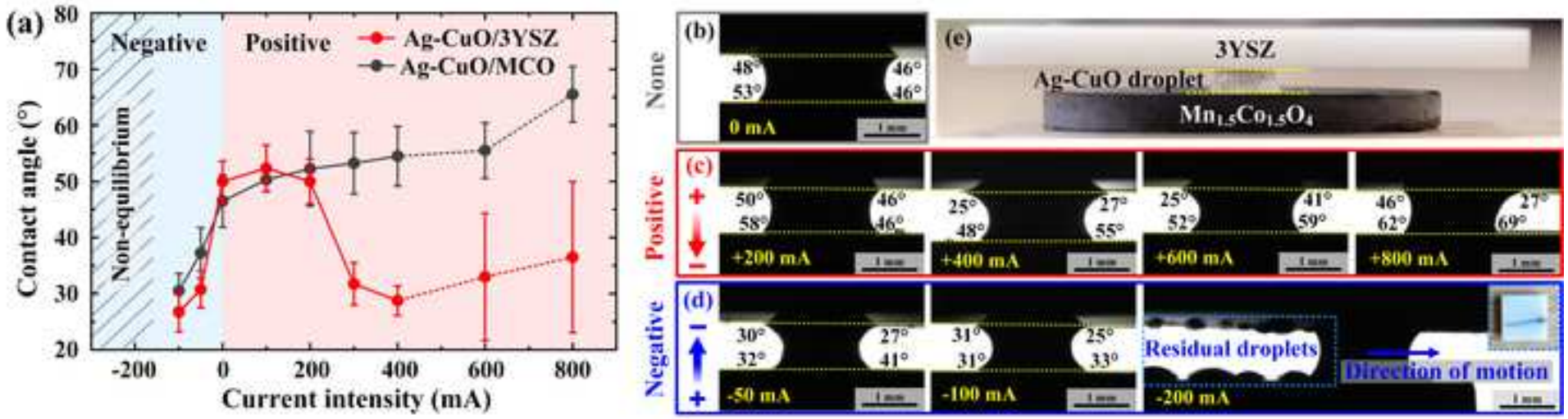

Figure 3

Click here to access/download;Figure;Fig. 3.jpg

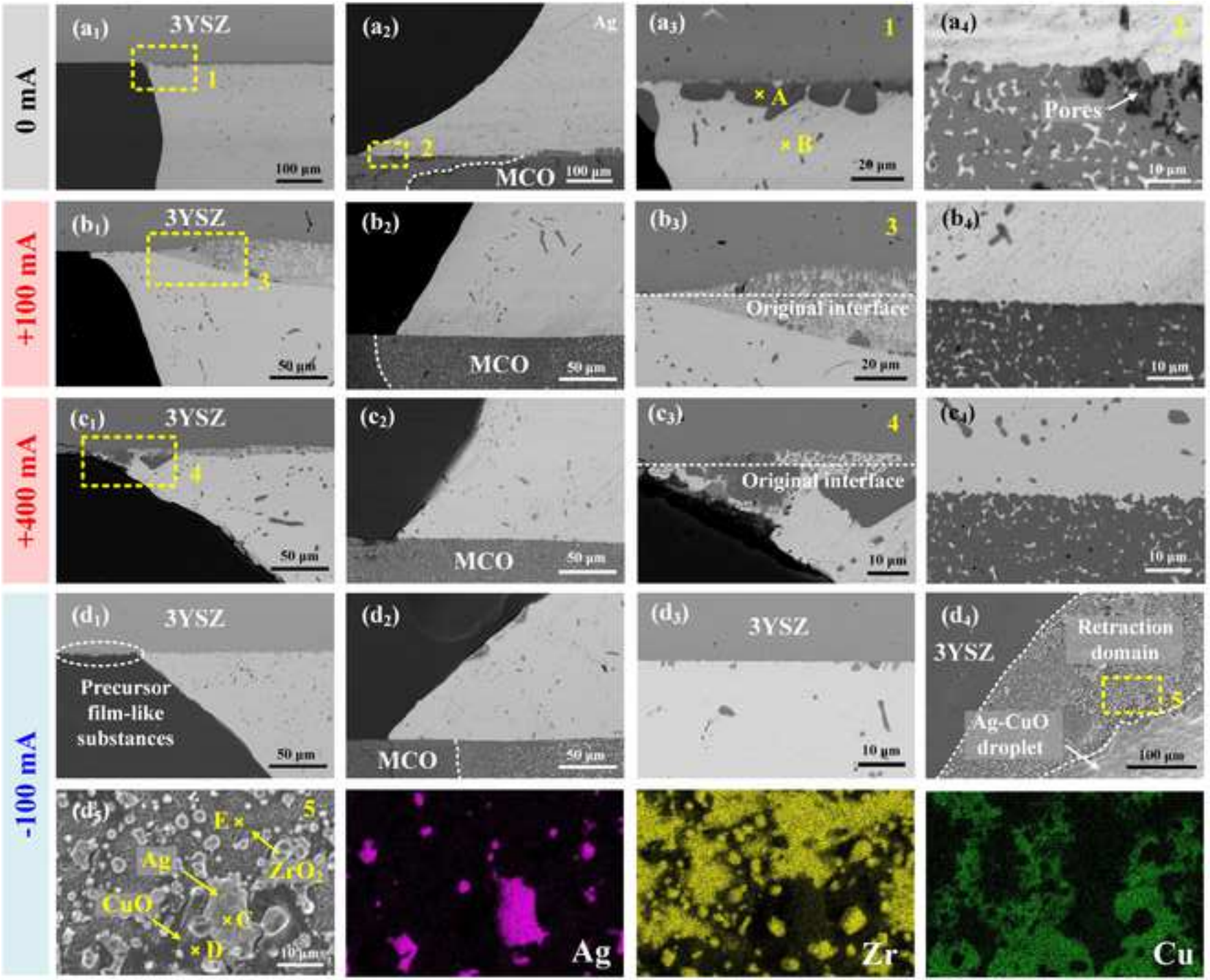

Figure 4

Click here to access/download;Figure;Fig. 4.jpg

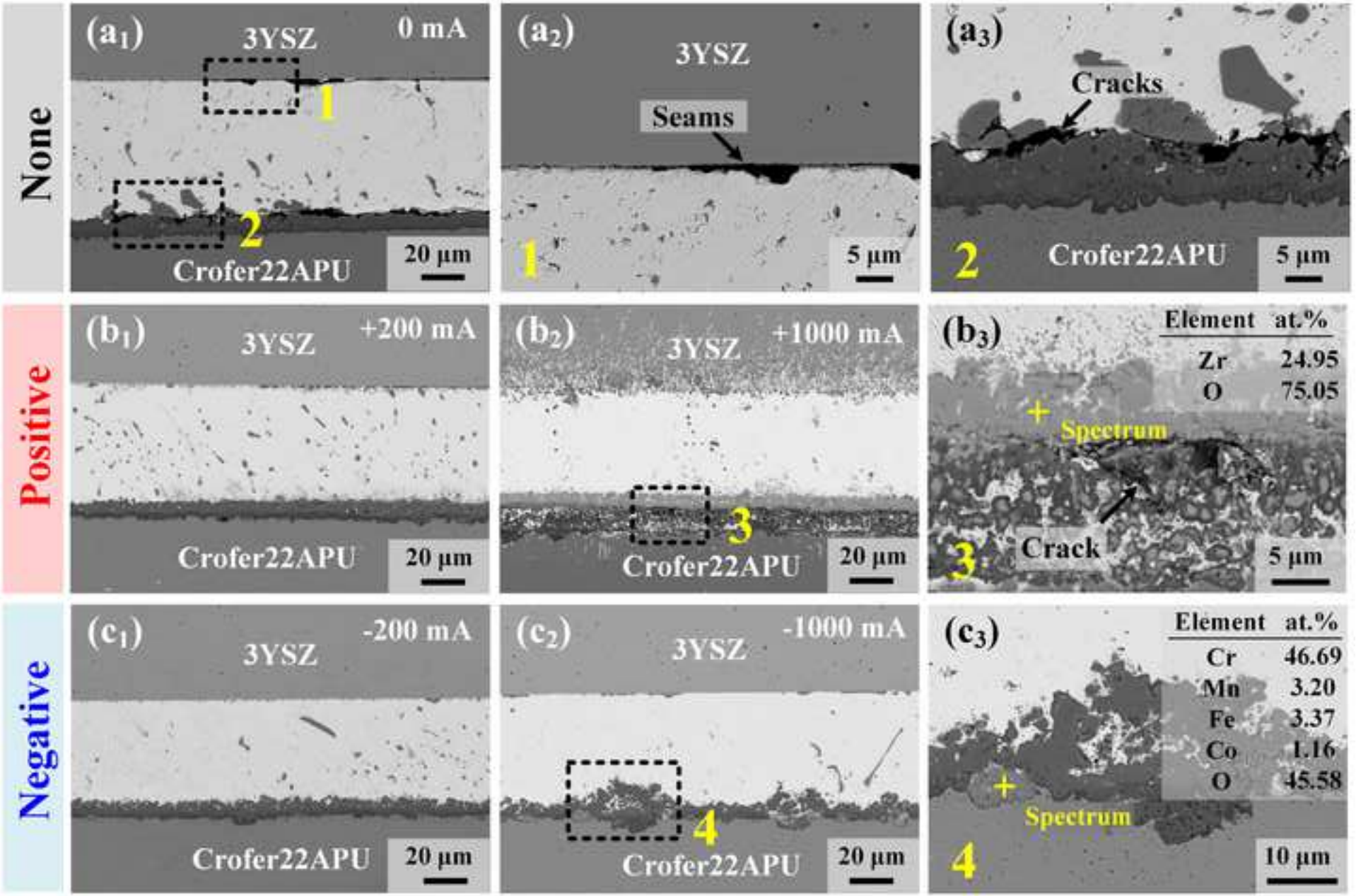

Figure 5

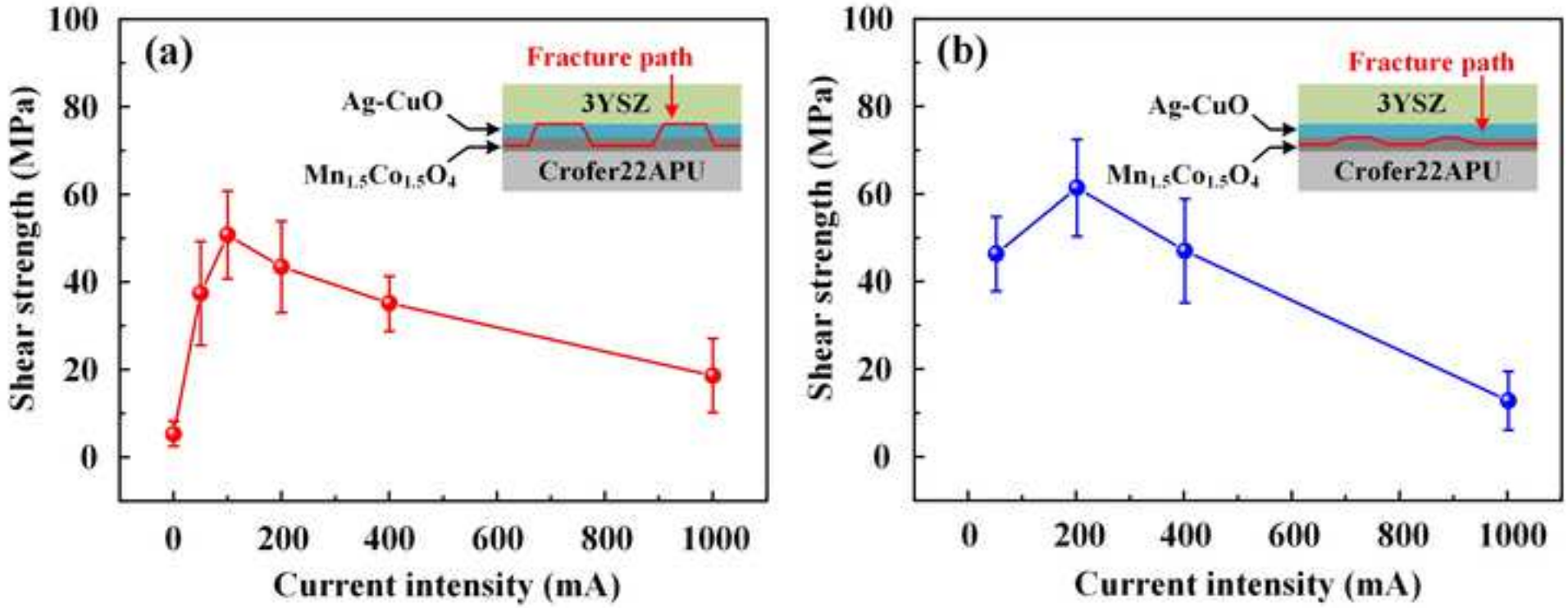

Figure 6

Click here to access/download;Figure;Fig. 6.jpg

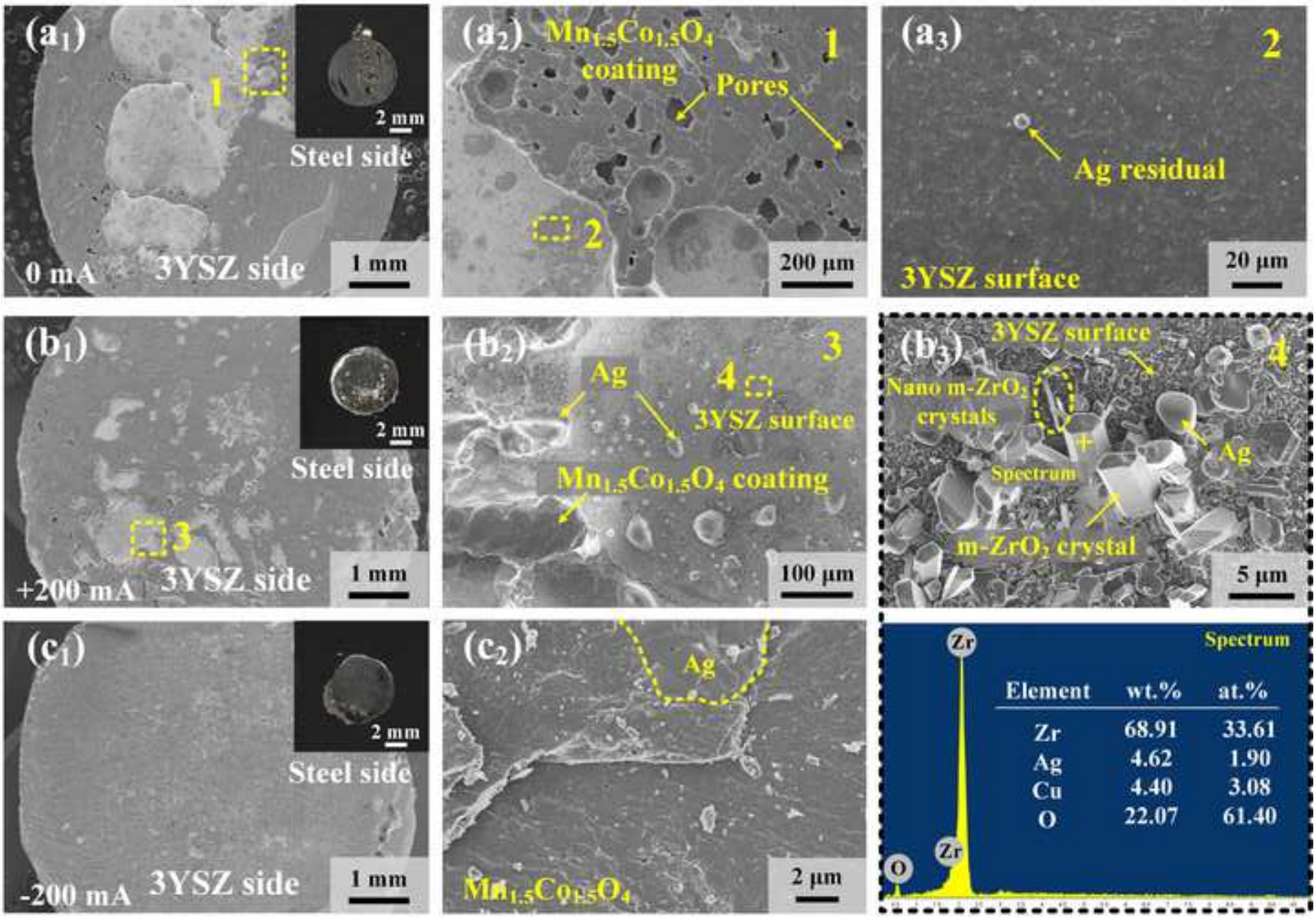

Figure 7

Click here to access/download;Figure;Fig. 7.jpg

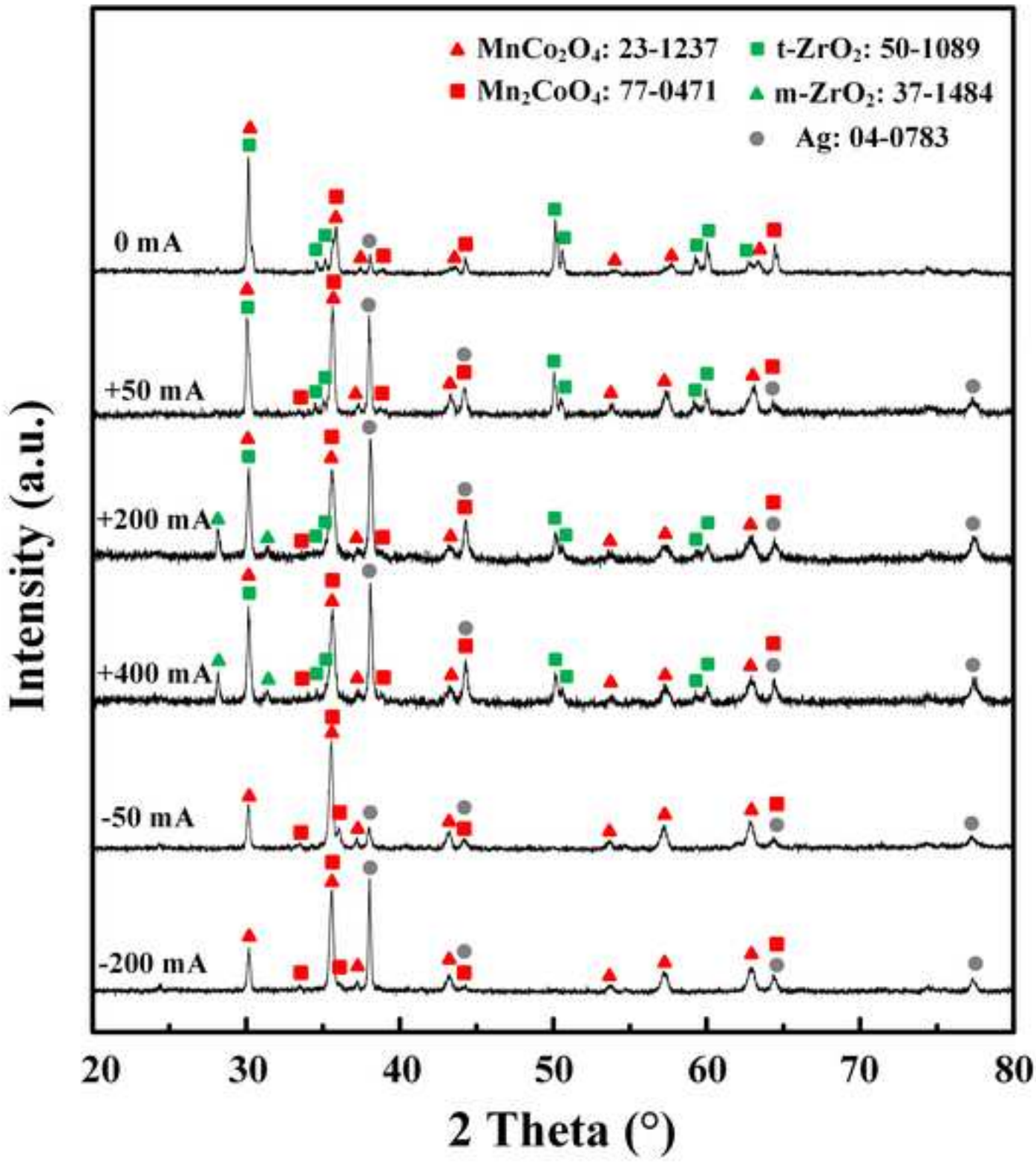

Figure 8